Czech Technical University in Prague
Faculty of Nuclear Sciences and Physical Engineering

Department of Physics
Field: Nuclear Engineering
Branch: Experimental nuclear physics

Charm quark production

BACHELOR'S THESIS

Author: Jitka Brabcová
Supervisor: Mgr. Jaroslav Bielčík, Ph.D.
Year: 2010

České vysoké učení technické v Praze
Fakulta jaderná a fyzikálně inženýrská

Katedra fyziky
Obor: Jaderné inženýrství
Zaměření: Experimentální jaderná fyzika

Produkce charm kvarku

BAKALÁŘSKÁ PRÁCE

Vypracoval: Jitka Brabcová
Vedoucí práce: Mgr. Jaroslav Bielčík, Ph.D.
Rok: 2010

Před svázáním místo téhle stránky vložíte zadání práce s podpisem děkana (bude to jediný oboustranný list ve Vaší práci) !!!!

Prohlášení

Prohlašuji, že jsem svou bakalářskou práci vypracovala samostatně a použila jsem pouze podklady (literaturu, projekty, SW atd.) uvedené v přiloženém seznamu.

V Praze dne ....

Poděkování

Děkuji Mgr. Jaroslavu Bielčíkovi, Ph.D. za vedení mé bakalářské práce a za podnětné návrhy, které ji obohatily.

Název práce: Produkce charm kvarku

Autor: Jitka Brabcová

Obor: Experimentální jaderná fyzika

Druh práce: Bakalářská práce

Vedoucí práce: Mgr. Jaroslav Bielčík, PhD.

Abstrakt: Těžké kvarky jsou produkované v počáteční fázi jádro-jaderné srážky a jsou proto citlivé na vlastnosti kvark-gluonového plazmatu. Dosud většina informací o produkci půvabných (c) a krásných (b) kvarků byla získána z nepřímých měření jejich semileptonických rozpadů. Přímé měření půvabných hadronů v jádro-jaderných srážkách může přinést přesnější informaci o jejich produkci a kolektivním toku.
Cílem práce je shrnout současné experimentální poznatky z měření půvabných hadronů na urychlovači RHIC a diskutovat jejich budoucí měření. Dále budou provedeny simulace produkce hadronů obsahujících půvabných kvark proton-protonových srážkách na urychlovači LHC.

Klíčová slova : Těžké kvarky, semileptonické rozpady charm a beauty, kvark-gluonové plazma, charmonium, účinný průřez, RHIC, LHC, detektor ALICE.

Title: Charm quark production

Author: Jitka Brabcová

Abstract: Heavy quarks are produced in early stage of nuclei-nuclei collisions thus they are sensitive to properties of quark-gluon plasma. The most of information about charm and beauty quark production have been received from indirect measurements their semileptonic decays. Direct measurements of charm hadrons in nuclei-nuclei collisions may serve more exact information about their production and collective flow.
Mean goal of this work is to conclude current experimental data of measurements charm hadrons on RHIC accelerator and discuss their further measurements. Next there will be completed simulation about hadron production contains charm quark in proton-proton collisions on LHC accelerator.

Key words: Heavy quarks, semileptonic decays for charm and beauty, quark-gluon plasma, charmonium, cross section, RHIC, LHC, ALICE detector.

Contents

List of Figures

Chapter 1

Introduction

In recent years nucleus-nucleus collision at high energy made important implications to fundamental understanding of nuclear matter. It is known that matter consists of quarks, leptons and particles of interactions. It is possible to create in laboratory conditions at large energy densities similar to these that existed in early phases of universe and in neutron stars.

The Relativistic Heavy Ion Collider (RHIC) is a heavy-ion collider located at and operated by Brookhaven National Laboratory (BNL) in Upton, New York. By using RHIC to collide ions traveling at relativistic speeds, physicists study the primordial form of matter that existed in the universe shortly after the Big Bang, and also the structure of protons.

RHIC was the most powerful heavy-ion collider in the world until the LHC went online and collided ions at higher energies in late 2009. It is also distinctive in its capability to collide spin-polarized protons.

In this thesis the production of heavy quarks in nucleus-nucleus collision is discussed. The main results of RHIC program are reported.

In chapter 2 are the Heavy ion physics and basic parameters discussed. In Chapter 3 there are fundamental information about the Quark-gluon plasma. In Chapter 4 there are the measuring facilities on LHC and ALICE detector discussed. In Chapter 5 there are experiments at RHIC discussed. In Chapter 6 there is the Open Heavy flavor discussed. In Chapter 7 is the Quarkonia measurement reported.

Chapter 2

Heavy ion physics

Heavy ion physics deals with nucleus-nucleus collision of high energy. The nuclear matter at conditions of high nuclear energy density can be created. Many calculations predict that at a critical temperature $T_c = 170MeV$, corresponding to an energy density $\epsilon_c = 1GeV/fm^3$, nuclear matter undergoes a phase transition to a deconfined state of quarks and gluons, called Quark-Gluon Plasma. Heavy-ion collisions are used to attain the energy density, exceeding ϵ_c. This makes the QCD (quantum chromodynamics) phase transition potentially realizable within the reach of the laboratory experiments.

In theoretical physics, quantum chromodynamics (QCD) is a theory of the strong interaction (color force), a fundamental force describing the interactions of the quarks and gluons making up hadrons. It has two main features. Asymptotic freedom, which means that the coupling constant α_s (this constant is describing the strong interaction) for the strong force becomes smaller at shorter distances. Confinement, which means that in normal conditions the free quarks do not exist. Because of this, it would take an infinite amount of energy to separate two quarks; they are forever bound into hadrons such as the proton and the neutron.

The objective is then to identify and to provide suitable QGP signatures, allowing to study the properties of QGP. To that end, a variety of observables (probes) can be used.

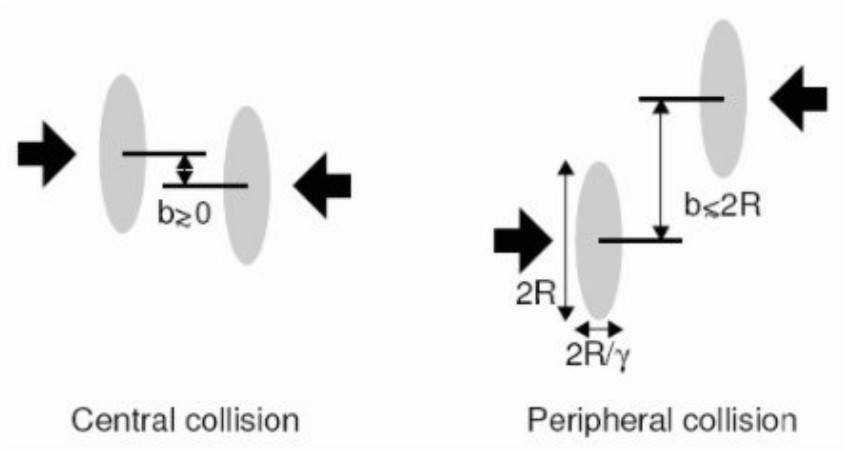

Figure 2.1: The central and peripheral collision

Firstly will be described the relativistic collision (Fig.2.1). According to minimum distance of two interacting nucleons there are two main categories - the central and the peripheral collision. On this figure b denotes the impact parameter. There can be seen when the impact parameter decreases (almost to zero) the collision becomes the most central and with the highest number of participants - nucleons in the overlap region participating on the collision.

The particle emission is asymmetrical, with the azimuthal anisotropies in momenta p_T perpendicular to the beam of various particles. The distribution of these momenta can be quantified by a Fourier decomposition and parametrized by the second Fourier coefficient - elliptical flow $v_2 =< cos2\phi >$ in which the angle ϕ is measured relative to the direction of impact and it can show us a p_T dependence.

The next effect characterizing the evolution of the collision is the nuclear modification factor R_{AA} defined as the ratio of the number of events at different values of p_T for gold-gold collisions normalized to the number of events in proton-proton collisions, scaled by the number of collisions N_{coll} .

$$R_{AA} = \frac{yield(Au + Au)}{yield(p + p) \times N_{coll}} \tag{2.1}$$

Hydrodynamics provides a simple, intuitive dynamic description of relativistic heavy ion collisions. Most of the experimental data on soft hadron production at RHIC are well described by ideal hydrodynamics. However, some problems remain. For example, one of the most important signals of collectivity, the elliptic flow, saturates beyond $p_T \approx 1.5 - 2GeV/c$ while ideal hydrodynamics predicts a continuous increase with p_T. Ideal hydrodynamic may not give an accurate description of the early stage of the collision. In the early stages of

collision, particle momenta are predominantly in the beam direction, while ideal hydrodynamic assumes a locally isotropic distribution. The anisotropy in the momentum distribution will give rise to shear viscous stress. Other dissipative effects, e.g. bulk viscosity and heat conduction can also affect the hydrodynamic evolution of QGP. Unlike ideal flow, non-ideal flow generates entropy. The space-time evolution is also changed. On the Fig.2.2 is shown the space-time evolution of the QGP with respect to hydrodynamics.

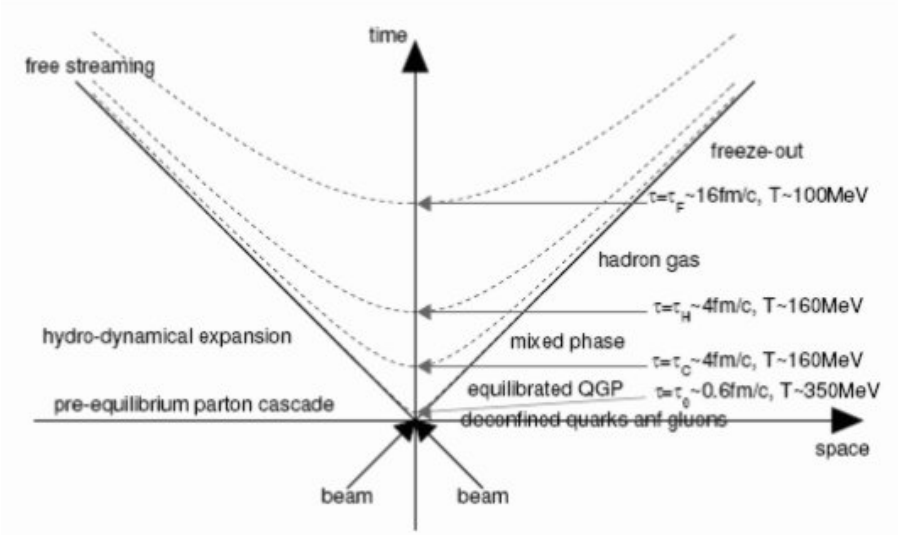

Figure 2.2: The space-time evolution of the QGP

Chapter 3

Quark-gluon plasma

A quark–gluon plasma (QGP) is a phase of quantum chromodynamics (QCD) which exists at extremely high temperature and/or density. This phase consists of (almost) free quarks and gluons. In hadron gas phase are partons confined.

The difference between these two phases of QCD is that in normal matter each quark either pairs up with an anti-quark to form a meson or joins with two other quarks to form a baryon (such as the proton and the neutron). In the QGP, by contrast, these mesons and baryons lose their identities and dissolve into a fluid of quarks and gluons. In normal matter quarks are confined; in the QGP quarks are deconfined. This matter does not behave as a quasi-ideal state of free quarks and gluons, but, rather, as an almost perfect dense fluid.

The QGP creation

The QGP can be created by heating matter up to a temperature of $2 \cdot 10^{12} K$, which amounts to 175 MeV per particle (the cross-over temperature from the normal hadronic to the QGP phase) and corresponding to an energy density of about 1 GeV/fm^3. This can be accomplished by colliding two large nuclei at high energy (note that 175 MeV is not the energy of the colliding beam).

Lead and gold nuclei have been used for such collisions at CERN SPS and BNL RHIC, respectively. The nuclei are accelerated to ultrarelativistic speeds and slammed into each other while Lorentz contracted. They largely pass through each other, but a resulting hot volume called a fireball is created after the collision. Once created, this fireball is expected to expand under its own pressure, and cool while expanding. By carefully studying this flow, experimentalists hope to put the theory to test.

A plasma is matter in which charges are screened due to the presence of other mobile charges. In a QGP, the color charge of the quarks and gluons is screened. The QGP has other analogies with a normal plasma but there are also dissimilarities. Outside a finite volume of QGP the color electric field is not screened, so that volume of QGP must still be color-neutral. It will therefore, like a nucleus, have integer electric charge.

Currently studied issues

QCD is one part of the modern theory of particle physics called the Standard Model. Other parts of this theory deal with electroweak interactions and neutrinos. Perturbative aspects of QCD have been tested to a few percent. In contrast, non-perturbative aspects of QCD have barely been tested. The study of the QGP is part of this effort to consolidate the grand theory of particle physics.

For relativistic matter, pressure and temperature are not independent variables, so the equation of state is a relation between the energy density and the pressure. Response functions such as the specific heat and various quark number susceptibilities are currently being computed.

The equation of state is an important input into the flow equations. The speed of sound is currently under investigation in lattice computations. The mean free path of quarks and gluons has been computed using perturbation theory. Lattice computations have been slower here, although the first computations of transport coefficients have recently been concluded. These indicate that the mean free time of quarks and gluons in the QGP may be comparable to the average interparticle spacing: hence the QGP is a liquid as far as its flow properties go. The incorporation of dissipative phenomena into hydrodynamics is another recent development that is still in an active stage.

Does the QGP really contain (almost) free quarks and gluons? The study of thermodynamic and flow properties would indicate that this is an oversimplification. It has been hypothesized recently that some mesons built from heavy quarks (such as the charm quark) do not dissolve until the temperature reaches about 350 MeV. This has led to speculation that many other kinds of bound states may exist in the plasma. Some static properties of the plasma (similar to the Debye screening length) constrain the excitation spectrum.

The important results of the measurement of the hot QCD matter created at RHIC are:

- Collective anisotropy, or elliptic flow. The transverse momentum p_T and the dependence of the elliptical flow v_2 is shown. The elliptical flow steadily increases with the transverse momentum (Fig.3.1).

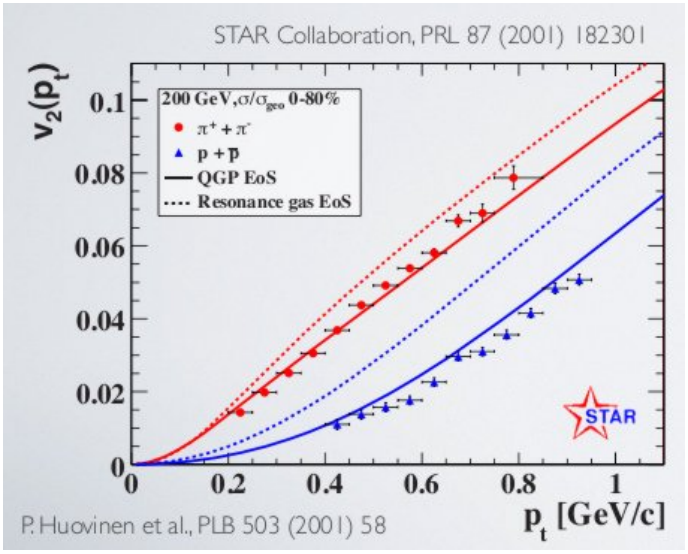

Figure 3.1: The elliptic flow

- Jet quenching. In the heavy ion collision event, scattering with a high transverse p_T can serve as a probe for the hot QCD matter, as it loses its energy while traveling through the medium. Experimentally, the quantity R_{AA} (A is the mass number) is the ratio of observed jet yield in A+A collisions and N_{bin} · yield in p+p collision (Fig.3.2).

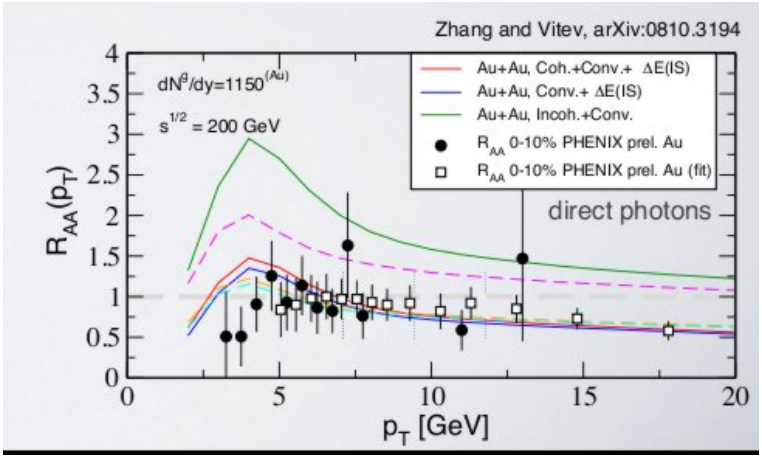

Figure 3.2: Energy loss

- Particle ratios. On the Fig.3.3 there are two significant effects shown. The particle ratios of the most central collisions are higher than of the peripheral collisions. The ratio has saturated value and it equals 1. The second effect is that ratio antiproton/pion is lower than proton/pion.

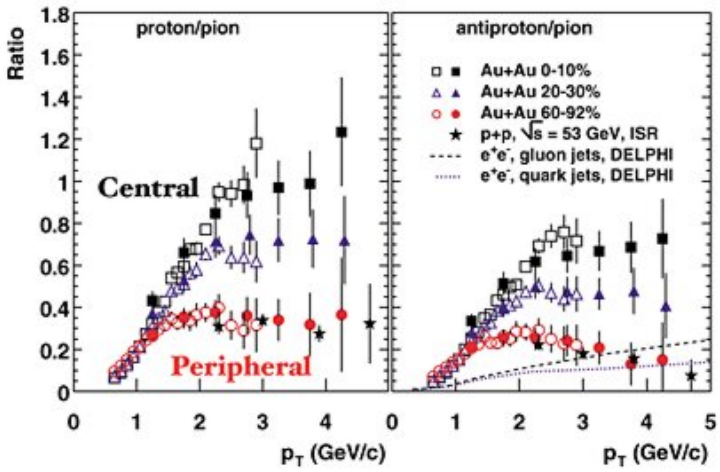

Figure 3.3: The particle ratios

- Di-hadron correlations. On Fig.3.4 is shown the yield dependency to angle of scattered Di-hadrons. Most of products from the collision spreads away under angles 0^o and 180^o for $p + p$ or $d + Au$, but peak at away side is suppressed for central $Au + Au$.

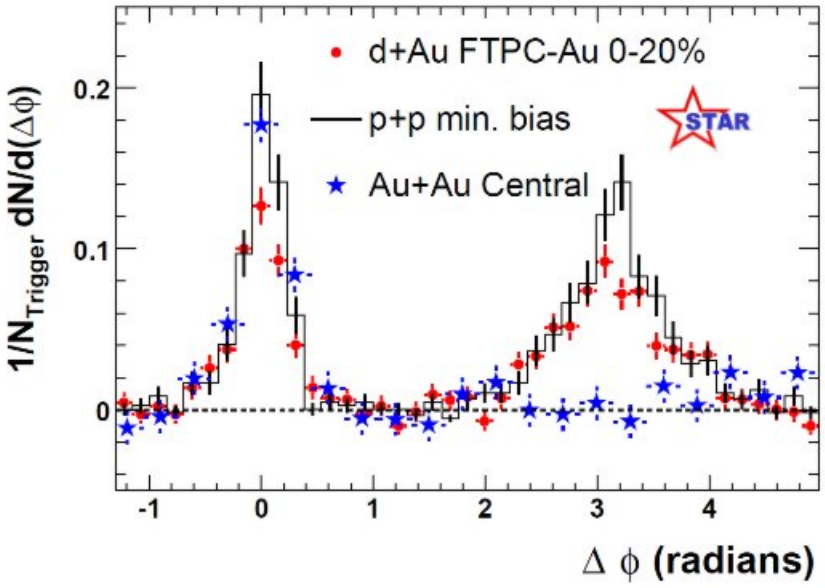

Figure 3.4: Di-hadron correlations

Other important measurement is J/ψ suppression that we discuss in Chapter 8.

In April 2005, formation of quark matter was tentatively confirmed by results obtained at Brookhaven National Laboratory's Relativistic Heavy Ion Collider (RHIC). This was summarized in papers from all RHIC experiment. The quark–gluon liquid of very low viscosity has been created.

Chapter 4

ALICE detector at LHC

The Large Hadron Collider (LHC) is the world's largest and highest-energy particle accelerator, a synchrotron intended to collide opposing particle beams of either protons at an energy of 7 TeV per particle, or lead nuclei at an energy of 574 TeV per nucleus.

The short history

On 27 March 2007 a cryogenic magnet support broke during a pressure test involving one of the LHC's inner triplet (focusing quadrupole) magnet assemblies, provided by Fermilab and KEK. Analysis revealed that its design, made as thin as possible for better insulation, was not strong enough to withstand the forces generated during pressure testing.

After many years at construction, LHC was started in 2008. Problems occurred on 19 September 2008 during powering tests of the main dipole circuit, when an electrical fault in the bus between magnets caused a rupture and a leak of six tonnes of liquid helium. The operation was delayed for several months. It is currently believed that a faulty electrical connection between two magnets caused an arc, which compromised the liquid-helium containment. Once the cooling layer was broken, the helium flooded the surrounding vacuum layer with sufficient force to break 10-ton magnets from their mountings. The explosion also contaminated the proton tubes with soot.

28 Feb 2010 the LHC continues operations ramping energies to run at 3.5 TeV for 18 months to two years, after which it will be shut down to prepare for the 14 TeV collisions (7 TeV per beam). 30 Mar 2010 the two beams collided at 7 TeV in the LHC at 13:06 CEST, marking the start of the LHC research program.

The ALICE detector

ALICE detector (Fig.4.1) is dedicated to investigating nucleus-nucleus collisions at an energy of 2,8 TeV (or more) per nucleon in each of the colliding nuclei. The main part of the apparatus in the solenoidal magnet, which regenerates a

field strength of 0,5 T within a volume of 1 600 m^3.

Various detectors are arranged in cylindrical shells around the interaction point. They determine an identity and precise trajectory of the more than 10 000 charged particles propelled by a Pb-Pb collision into the active volume of the apparatus. The innermost detector is the inner tracking system (ITS), which consists of six layers of silicon detectors surrounding the 1-mm-thick beam pipe that encloses ultra-high vacuum of the accelerator. These detectors determine e.g.the decay vertex of short-lived particles carrying strange, charm or bottom quantum numbers that typically decay within a few millimetres to centimetres of the primary interaction point.

The ITS is contained within, and mounted on, the cylindrical barrel of the time projection chamber (TPC). This is ALICE's major tracking device provides essentially continuous, three-dimensional tracking of charged particles between radii of 80 cm and 250 cm from the central interaction point.

Outside the TPC there are two very large (with areas about 150 m^2) particle identification detectors: 1) the transition radiation detector (TRD) for the triggering and identifying of electrons, 2) the time-of-flight (TOF) detector which can record the transit time between the interaction point and the detector surface at a resolution of better than 100 picoseconds.

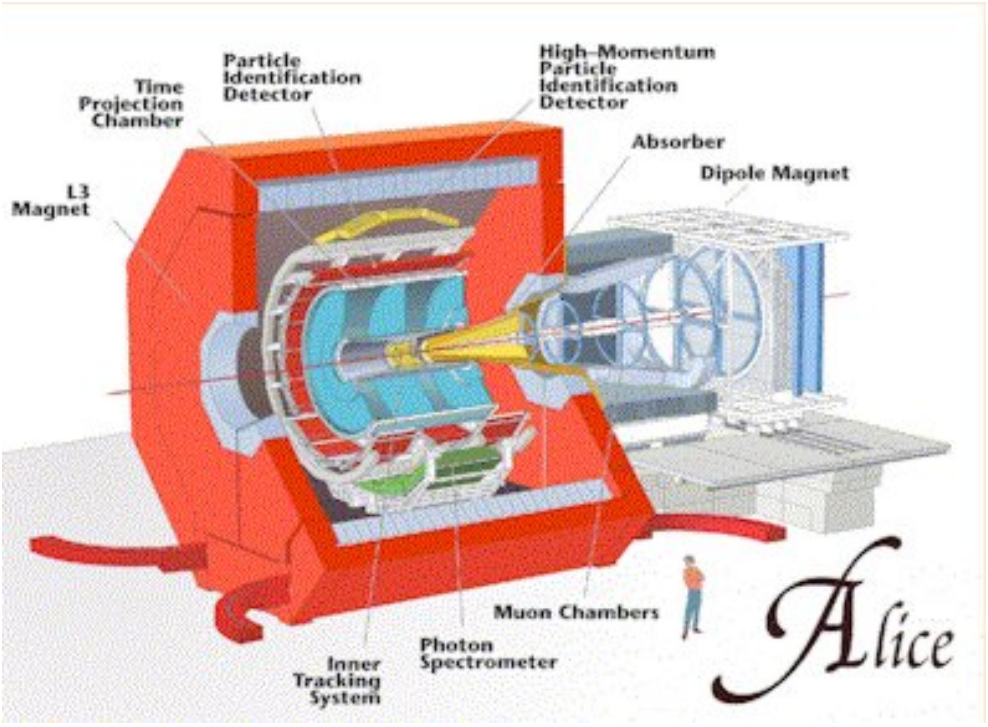

Figure 4.1: ALICE

The central barrel of ALICE is completed by dedicated detectors to measure photons (PHOS) and their distribution in the forward direction (PMD) and to identify high-momentum hadrons (HMPID), and by further detectors to determine the position and time of the primary interaction point.

Separated from the main detector in the forward direction of one of the accelerator beams, and behind a conical absorber that projects into the central barrel, is a muon detector with its own large dipole magnet. Because muons do not undergo strong reactions and do not emit bremmstrahlung, they penetrate the absorber practically unscathed- unlike hadrons. Their momenta are then measured in tracking station before, inside, and after the dipole magnet.

On the Fig.4.2 there is an examples of the measurement on ALICE detector. The $p + p$ and $Pb + Pb$ collisions are needed.

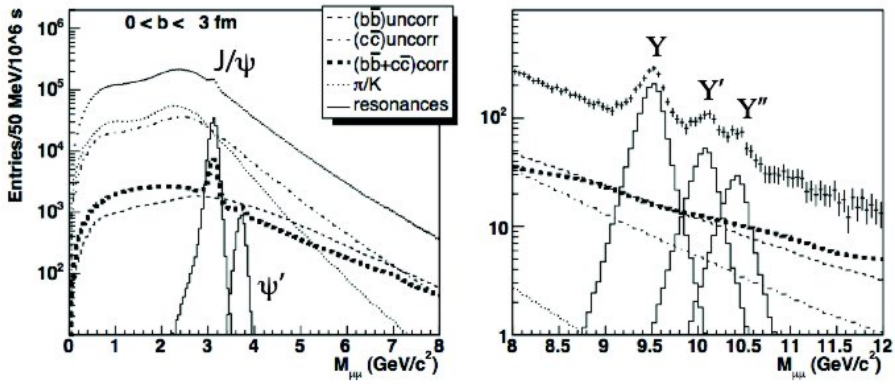

Figure 4.2: The J/ψ and Υ measured in forward rapidity via muon channel

Other detectors

ATLAS - one of two general purpose detectors. ATLAS will be used to look for signs of new physics, including the origins of mass and extra dimensions.

CMS - the other general purpose detector will, like ATLAS, hunt for the Higgs boson and look for clues to the nature of dark matter.

LHCb - equal amounts of matter and antimatter were created in the Big Bang. LHCb will try to investigate what happened to the "missing" antimatter.

Chapter 5

Experiment at RHIC

RHIC is the first machine in the world, the intersecting storage ring particle accelerator capable of colliding heavy ions. Two independent rings allow a virtually free choice of colliding projectiles. RHIC primarily uses ions of gold, one of the heaviest common elements, because its nucleus is densely packed with particles. On the Fig.5.1 there is a simple schematic of the RHIC and its detectors.

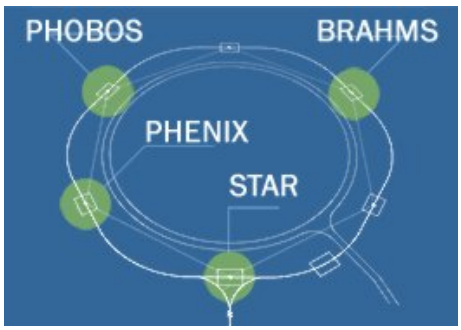

Figure 5.1: RHIC detectors

RHIC double storage ring is itself hexagonally shaped and 3834 m long in circumference, with curved edges in which stored particles are deflected by 1,740 superconducting niobium-titanium magnets. The dipole magnets operate at 3.45 teslas. The six interaction points are at the middle of the six relatively straight sections, where the two rings cross, allowing the particles to collide.

There are four detectors at RHIC: STAR (6 clock, and near the ATR), PHENIX (8 clock), PHOBOS (10 clock), and BRAHMS (2 clock). Two of them are still active, with PHOBOS having completed its operation after 2005 and Run-05, and BRAHMS after 2006 and Run-06.

Sitting on the 8 o'clock interaction point is the PHENIX detector. The

Central magnet in the interaction region with the beam pipe is in its center. To the right is in an extracted position, the East Carriage with the ring imaging Cherenkov detector (RICH).

A particle passes through several stages of boosters before it reaches the RHIC storage ring. Firstly are ions in the Tandem Van de Graaff accelerated, while for protons, the 200 MeV linear accelerator (Linac) is used. As an example, gold nuclei leaving the Tandem Van de Graaff have an energy of about 1 MeV per nucleon and have an electric charge Q = +32 (32 electrons stripped from the gold atom). The particles are then accelerated by the Booster Synchrotron to 95 MeV per nucleon, which injects the projectile now with Q = +77 into the Alternating Gradient Synchrotron (AGS), before they finally reach 8.86 GeV per nucleon and are injected in a Q = +79 state (no electrons left) into the RHIC storage ring over the AGS-To-RHIC Transfer Line (ATR), sitting at the 6 o'clock position.

The main types of particle combinations used at RHIC are p+p, d+Au, Cu+Cu and Au+Au. The projectiles typically travel at a speed of 99.995% of the speed of light in vacuum. For Au+Au collision, the center-of-mass energy $\sqrt{s_{NN}}$ is typically 200 GeV (or 100 GeV per nucleon); a luminosity of $2 \cdot 10^{26} cm^{-2} \cdot s^{-1}$ was targeted during the planning. The current luminosity performance of the collider is $2,96 \cdot 10^{26} cm^{-2}$ s^{-1} (Run-4). For $p + p$ collision, Run-9 achieved center-of-mass energy of 500 GeV at February 12, 2009[1].

One unique characteristic of RHIC is its capability to produce polarized protons. RHIC holds the record of highest energy polarized protons. Polarized protons are injected into RHIC and preserve this state throughout the energy ramp. First gold ion beam-beam collisions at a momentum of 100+100 GeV/c per nucleon on STAR showing hadronized charged particle debris curving in the magnetic field of the instrument.

STAR is aimed at the detection of hadrons with its system of time projection chambers covering a large solid angle and in a conventionally generated solenoidal magnetic field. PHENIX is further specialized in detecting rare and electromagnetic particles, using a partial coverage detector system in a superconductively generated axial magnetic field.

PHOBOS has the largest pseudorapidity coverage of all detectors, and tailored for bulk particle multiplicity measurement. BRAHMS is designed for momentum spectroscopy. There is an additional experiment PP2PP, investigating spin dependence in p+p scattering.

Chapter 6

Open Heavy Flavor

This chapter will report about observations of hadrons containing c or b quark, mainly D-mesons and non-photonic electrons from semileptonic decays of D and B hadrons. The cross section, rapidity dependence and the nuclear modification factor will be also shown. Open heavy flavor hadrons are particles that contains one c ($\bar{c}$) or b ($\bar{b}$) quark. Total charm quantum number is non-zero. Oppositely the Hidden Heavy Flavor known as Quarkonia - J/ψ, Υ is a bound state of $c\bar{c}$ or $b\bar{b}$, so their charm or beauty quantum number is zero.

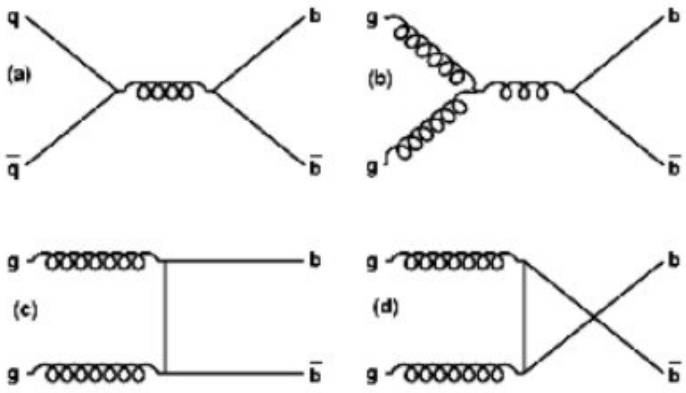

Figure 6.1: Feynmann diagram representing c, b production mechanisms

On Fig.6.1 the most important Feynmann diagrams of c, b production mechanism are shown. There are two gluons undergoing so called gluon fusion (b, c ,d) then it decays into charm (bottom pair). Or the $c\bar{c}$ could be produced by another pair of the quark and antiquark by the anihilation firstly convert to gluon (a). These mechanisms are analogical for b and c quark.

On Fig.6.2 the quark composition of several charm and beauty hadrons is shown together with the most important decays.

Particle	Mass [MeV/c²]	Quark content	Decay mode	Branching ratio
D^+	1 870	$c\bar{d}$	$\overline{K}^0$ anything+K^0 anything	(61 ± 5) %
			$\overline{K}^0\mu^+\nu_\mu$	(9.3 ± 0.8) %
			$\overline{K}^0e^+\nu_e$	(8.6 ± 0.5) %
D^0	1 865	$c\bar{u}$	K^- anything	(54.7 ± 2.8) %
			$\overline{K}^0$ anything+K^0 anything	(47 ± 4) %
			$K^-e^+\nu_e$	(3.58 ± 0.06) %
Λ_c^+	2 287	udc	$pK^-\pi^+$	(5.0 ± 1.3) %
			$\Lambda e^+\nu_e$	(2.1 ± 0.6) %
			$\Lambda\mu^+\nu_\mu$	(2.0 ± 0.7) %
B^0	5 280	$d\bar{b}$	$l^+\nu_l$ anything	(10.33 ± 0.28)%
			$e^+\nu_eX_c$	(10.1 ± 0.4)%
			$Dl^+\nu_l$ anything	(9.6 ± 0.9)%
$B^{+(-)}$	5 279	$u\bar{b}(\bar{u}b)$	$l^+\nu_l$ anything	(10.99 ± 0.28)%
			$e^+\nu_eX_c$	(10.8 ± 0.4)%
			$Dl^+\nu_l$ anything	(10.4 ± 0.8)%

Figure 6.2: D-meson, Λ_c, B^0, B^- and B^+ decay modes

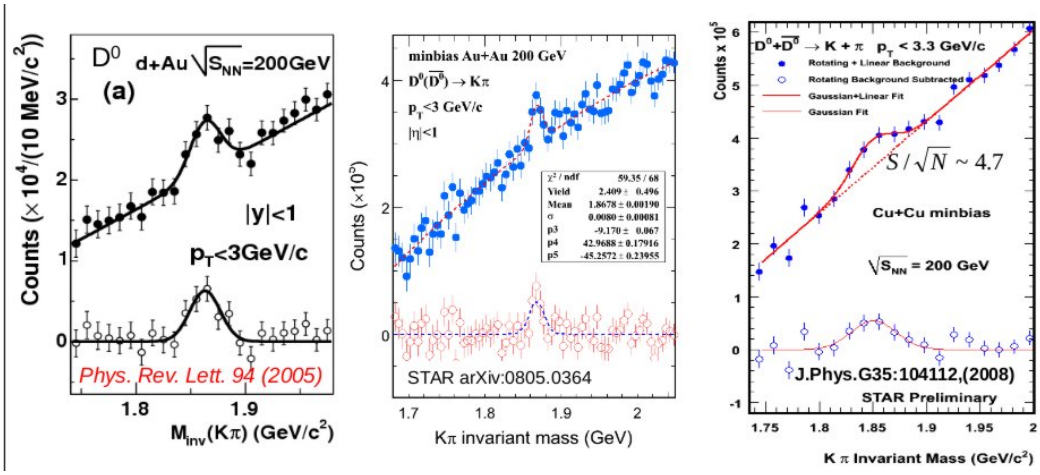

Figure 6.3: D^0-meson reconstruction in STAR, in d+Au, Au+Au and Cu+Cu collision at $\sqrt{s_{NN}} = 200GeV$

On the Fig.6.3 the direct measurement of D^0 meson performed by STAR ex-

periment in several collision system is shown. The decay used for reconstruction is $D^0 \rightarrow \mathrm{K}^- + \pi^+$, $\bar{D^0} \rightarrow \mathrm{K}^+ + \pi^-$.

In upper part invariant masses of $K^+\pi^-$ pairs is shown without subtraction at random combinatorial background. In lower part the mass peak is shown after subtraction of linear background. The figure shows D^0 measurement in d+Au (left), Au+Au (middle) and Cu+Cu (right) collisions at $\sqrt{s_{NN}} = 200GeV$.

The D^0 yield is fitted by a Gaussian peak plus a linear or second-order polynomial to describe the residual background to the measured distribution (red curve). The total systematic uncertainty on D^0 yield bin-by-bin is $\approx 40 - 50\%$, evaluated by varying the particle identification conditions and yield extraction procedures.

Fig.6.4 illustrates the p_T distributions of D^0 mesons for $d+Au$ and $Au+Au$ collisions. Red and blue dashed curves are power-law combined fit for D^0 and leptons. The gray boxes are bin-to-bin systematic uncertainties.

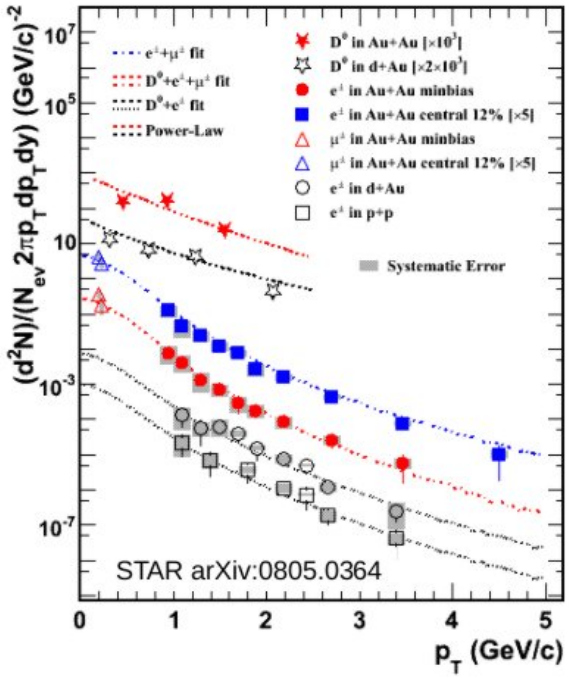

Figure 6.4: p_T-dependence for STAR charm quark measurement

Dashed lines indicate combine fit of D, μ and e^- STAR measurement used to extract total charm cross section. PHENIX uses only fit of non-photonic electron to extract of.

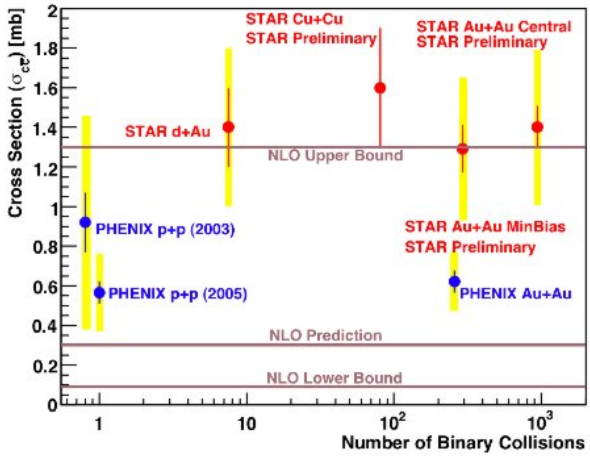

Figure 6.5: Open charm cross section compared for STAR and PHENIX measurement

The total charm cross section is a crucial input to models that incorporate regeneration of J/ψ in QCD matter via coalescence. In order to test these models, the charm cross section needs to be known with precision. Theoretical guidance is not strong, since as shown in Fig.6.5 the uncertainty in the calculated cross section ranges over nearly an order of magnitude.

Both PHENIX and STAR have made equivalent measurements in Au+Au collisions, where the STAR measurements additionally contain identified muons at extremely low p_T. Within STAR and PHENIX separately, the total charm cross section is found to scale well with the number of binary collisions, as expected if charm is produced in initial hard scatterings in Au+Au collisions, but there is a discrepancy of approximately a factor of 2 between the experiments. Both sets of measurements are consistent with theoretical calculations, within the large theoretical uncertainty [2].

Fig.6.6 and Fig.6.7 energy loss for charm, bottom and light quarks is shown. On Fig.6.6 there is a quantification dead cone effect for the heavy quark energy loss. On Fig.6.7 nuclear modification factor of the heavy and light quarks is shown. It seems that light quarks have constant value of the ratio for the whole p_T-range, meanwhile the charm and bottom quark's ratios decrease.

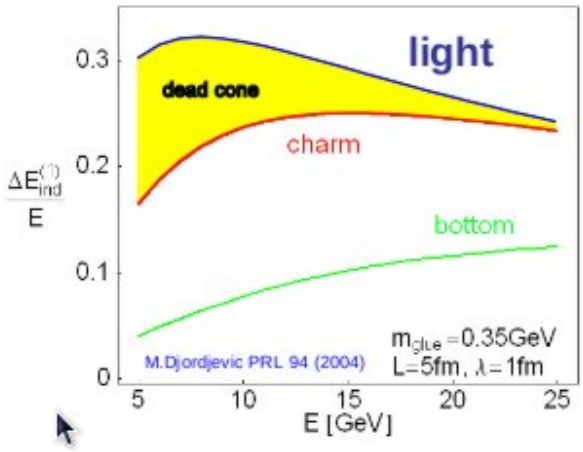

Figure 6.6: Energy loss for the light, charm and bottom quarks

The dead cone effect is a product of the heavy quark radiation. Gluon bremsstrahlung off a heavy-quark differs from the case of a massless parton (produced in a process with the same hardness scale) in one respect: gluon radiation is suppressed at angles smaller than the ratio of the quark mass M to its energy E.

Suppression of small-angle radiation has these implications: perturbative calculability of the heavy-quark fragmentation functions, multiplicity and energy spectra of light particles accompanying hard production of a heavy quark.

In summary smaller energy loss of charm and bottom quark results in larger value of R_{AA}. At some value of p_T the mass effect will become small.

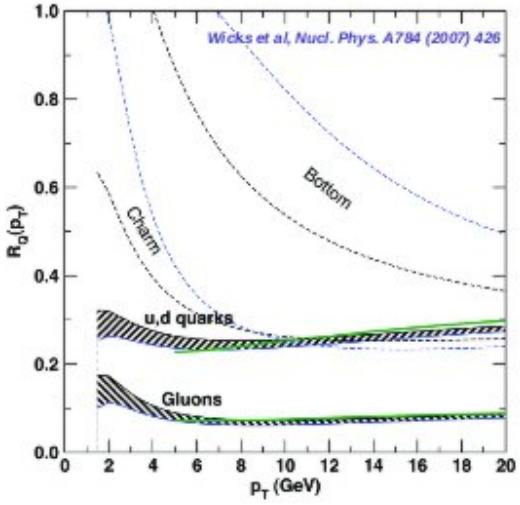

Figure 6.7: Comparison bottom and charm quark ratio to u,d quarks and gluons

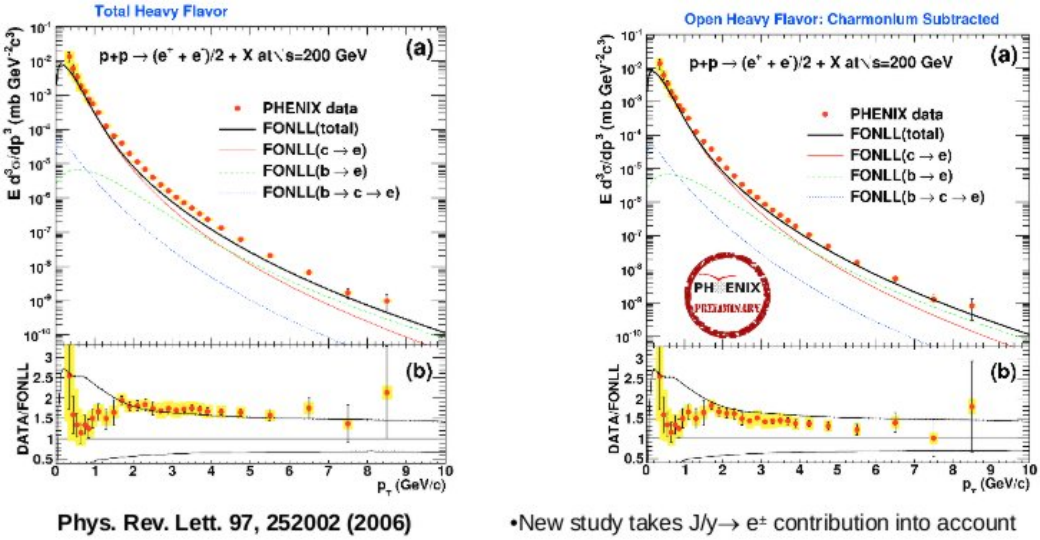

Figure 6.8: PHENIX charm measurement for Total Heavy Flavor and Open Heavy Flavor

Other measurement of charm and beauty is done via semileptonic decays of D

or B. Always contribution from other background electron has to be subtracted. Resulted sample is called non-photonic electron. On Fig.6.8(a) measurement of non-photonic electron for PHENIX is shown. The error bars (bands) represent the statistical (systematic) errors. The curves are the FONLL calculations.(b) Ratio of the data and the FONLL calculation. The upper (lower) curve shows the theoretical upper (lower) limit of the FONLL calculation. In both panels a 10% normalization uncertainty is not shown. All background has been subtracted.

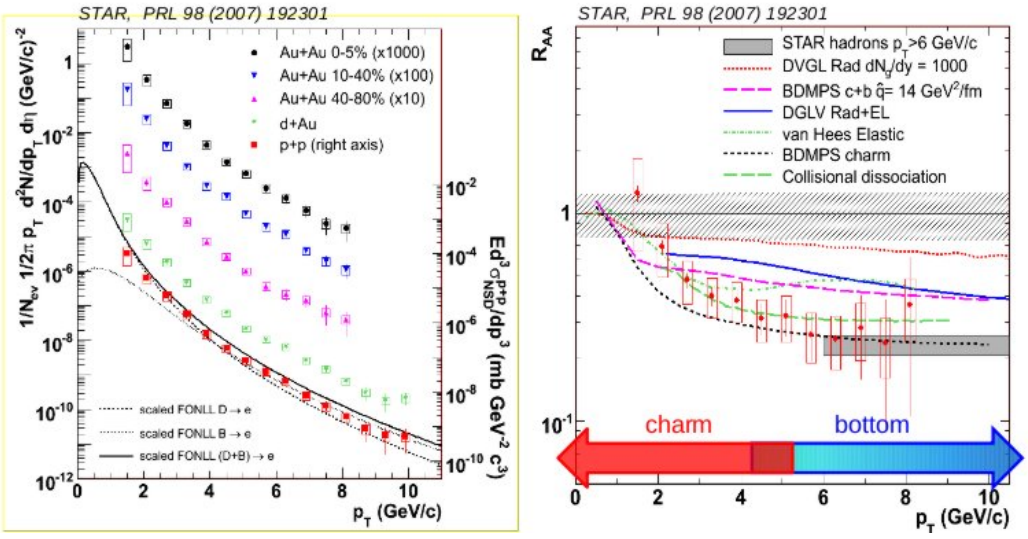

Figure 6.9: Suppression for non photo-electronic particles

On Fig.6.9 suppression for non photo-electronic particles in STAR is shown. The left panel describes the p_T-dependence of yields for several centralities in Au-Au collisions and the comparison to d-Au and p-p collisions (dots). The curves- dashed and solid show the scaled FONLL calculations. The right panel compares charm and bottom results for R_{AA}.

The curves show various theoretical calculation. At low p_T the dominant contribution is for c decays and at p_T $5GeV$ the bottom decay starts to be important. Shaded area shows suppression of inclusive hadrons (represents light partons).

Surprisingly R_{AA} of non photonic electron is similar to it. This is in contrast to expectations for dead cone effect. Therefore theoretical models cannot describe the observed suppression satisfactory, when both c, b contribution are taken into account.

Chapter 7

Quarkonia measurement

This chapter deals with quarkonia, mesons consisting from $c\bar{c}$ or $b\bar{b}$ quarks. The most important are J/ψ ($c\bar{c}$) and Υ ($b\bar{b}$). We will show in more detail their transverse momentum dependence and rapidity dependence of the modification factor. The comparison between the data from various experiments will be done.

Quarkonia are the bound states of heavy quark-antiquark pairs and decay electromagnetically to lepton pairs of invariant mass: the pair has the invariant mass of the decaying bound state.

J/ψ history

Quarkonia measurements are necessary for understanding production mechanism. The J/ψ is a subatomic particle, a flavor-neutral meson consisting of a charm quark and a charm antiquark ($c\bar{c}$). It was observed in 1974 at Stanford at SPEAR collider via e^+e anihilation, by Burton Richter and also at Brookhaven National Laboratory at the alternating gradient synchrotron (AGS) in $p + Be$ collisions, by Samuel Ting. This new particle decayed slowly and did not fit into the framework of up, down, and strange quarks. The J/ψ observation was the first experimental evidence for the fourth quark- charm.

Mesons formed by a bound state of a $c\bar{c}$ are generally known as "charmonium". The J/ψ is the first excited state of charmonium (i.e, the form of the charmonium with the second-smallest rest mass). The J/ψ has a rest mass of $3096,9MeV/c^2$, and a mean lifetime of $7,2.10^{-21}s$. This lifetime was about a thousand times longer than expected.

Quarkonia levels

Quarkonia can exist in several bound states creating quarkonia levels. At $T = 0$ the quarkonium bound energy spectra can be express by formula for nonrelativistic potential,

$$V(r, T = 0) = \sigma r - \frac{\alpha_c}{r} \tag{7.1}$$

where r is the separation between the Q and $\bar{Q}$. The $1/r$ is Coulomb-like term and governs the short distance behavior of the potential. It arises from the exchange of a gluon between the Q and $\bar{Q}$. The factor α_c can be related to the strong coupling constant to account for summation over color indices and σ is the string tension which determines the strength of the confining term.

The quarkonium levels can be calculated by solving the Schrodinger equation with the potential in Eq.(1). The binding energy, E_b, is related to the quarkonium mass, M, by

$$M = 2m_Q + E_b \tag{7.2}$$

where m_Q is the heavy quark mass. Because the potential has both positive and negative components, E_b can be either positive or negative. It depends on the value of m_Q relative to the mass of quarkonium state. Below are displayed values of the parameters that they best fit the general features of the spectrum.

$\sigma = 0.192GeV^2$, $\alpha_c = 0.471$, $m_c = 1.32GeV$, $m_b = 4.75GeV$.

There are on the Fig.7.1 and Fig.7.2 Charmonium and Bottomonium families with their quantum numbers. The thick transition lines indicate hadronic feed-down decays while the thinner lines indicate radiative decays. Unconfirmed states are shown as dashed lines. For Charmonium family there is $D\bar{D}$ threshold and for the Bottomonium family there is $B\bar{B}$ threshold.

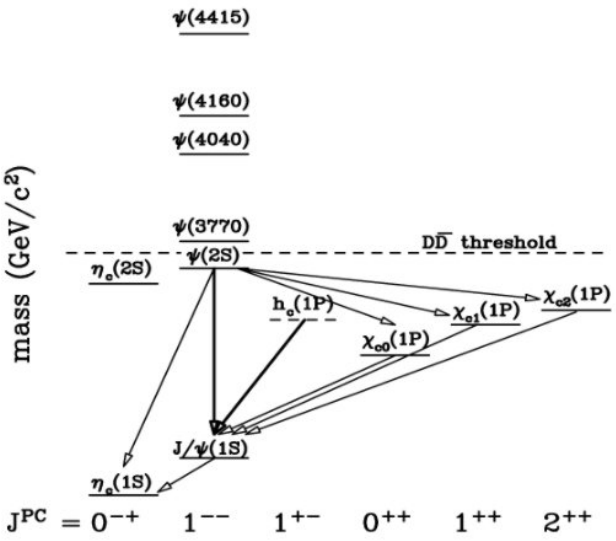

Figure 7.1: Charmonium family

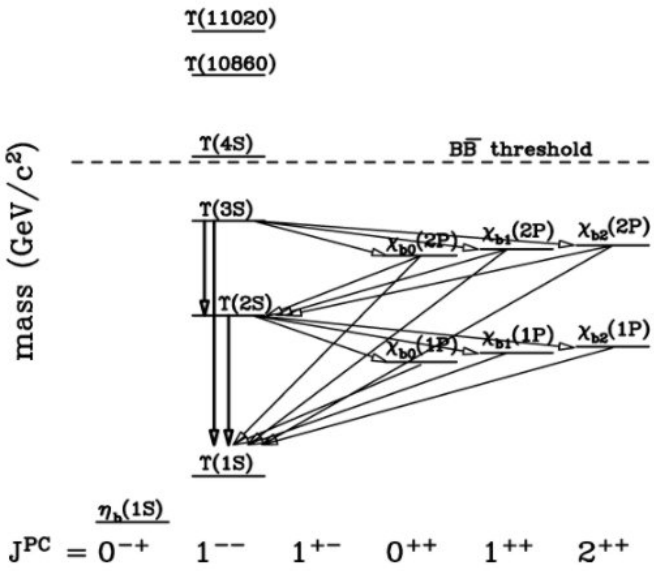

Figure 7.2: Bottomonium family

In Fig.7.3 an illustration of the OZI rule in charmonium decays can be seen. The OZI rule explains why certain decay modes appear less frequently than may be expected. Any strongly occurring process with a Feynman diagram that can be split in two by cutting only internal gluon lines will be suppressed. The OZI rule can be explained from the fact that the coupling constant in QCD decreases with increasing energy.

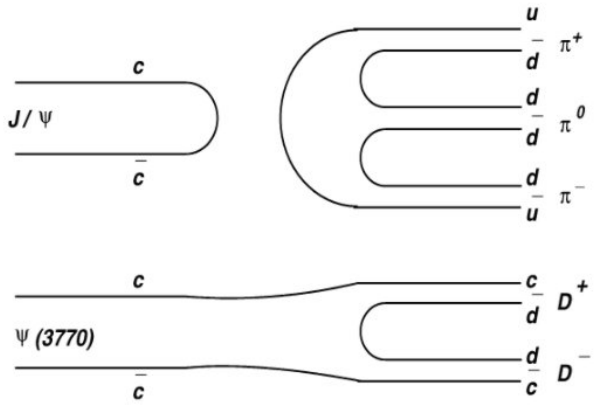

Figure 7.3: The OZI rule

Decays of J/ψ to hadrons are OZI suppressed since the quark lines are disconnected. Charmonium states below the $D\bar{D}$ threshold are forced to annihilate to gluons to decay to lighter hadrons. Decays to charm mesons with connected quark lines, possible for the $\psi(3770)$, is OZI favored. The differences in the decay channels can be described empirically.

J/ψ melting and decay modes

In a hot QCD medium, when the temperature is raised well beyond the critical temperature, the J/ψ and its excitations are expected to melt due to color screening of bounding potential [16]. This is one of the predicted signals of the formation of the quark-gluon plasma. It has been studied in Heavy-ion experiments at CERN's Super Proton Synchrotron and at BNL's Relativistic Heavy Ion Collider. The disappearance of J/ψ mesons is evaluated with respect to the baseline provided by the total production of all charm quark-containing subatomic particles is required. It is also expected that some of the J/ψ are produced and/or destroyed at time of QGP hadronization. Thus there is uncertainty in the prevailing conditions at the initial collisions.

Instead of suppression, enhanced production of J/ψ is expected [17] in heavy ion experiments at LHC where the quark-combinant production mechanism should be dominant given the large abundance of charm quarks in the QGP. Aside of J/ψ, charmed B mesons (B_c), offer a signature that indicates that quarks move freely and bind at-will when combining to form hadrons.[18] [19]

The hadronic decay modes of the J/ψ are strongly suppressed. This effect increases the lifetime of the particle and it is the consequence coming from the weak decay. Therefore it gives its very narrow decay width of just $93,2 \pm 2,1 keV$ (Fig.7.4). Because of this strong suppression electromagnetic decays begin to compete with hadronic decays. This is why the J/ψ has a significant branching fraction to leptons.

Particle	Mass [MeV/c^2]	Width[MeV/c^2]	Decay mode	Branching ratio
			hadrons	87.7±0.5
J/ψ	3097	0.093	e^+e^-	5.94±0.10
			$\mu^+\mu^-$	5.93±0.10
χ_0	3415	10.4	J/$\psi + \gamma$	1.30±0.10
χ_1	3511	0.89	J/$\psi + \gamma$	35.6±1.9
χ_2	3556	2.06	J/$\psi + \gamma$	20.2±1.0
			hadrons	97.9±0.3
ψ'	3686	0.277	J/$\psi + X$	56.1±0.9
			e^+e^-	0.74±0.18
			$\mu^+\mu^-$	0.73±0.18

Figure 7.4: J/ψ decay modes

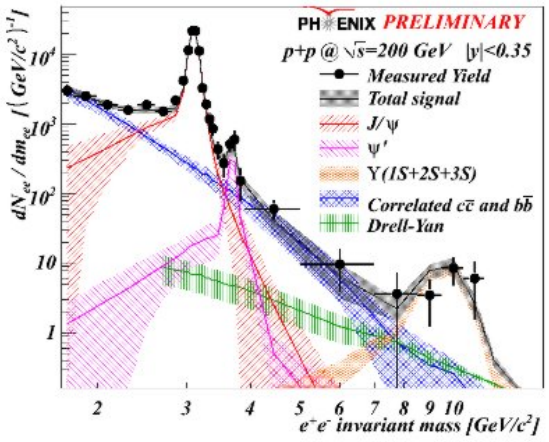

Figure 7.5: Invariant mass distribution

On Fig.7.5 the invariant mass spectrum of electron-positron pairs (somewhere is used dielectron) measured during the 2006 RHIC RUN (black dots) by PHENIX experiment. The combinatorial background was subtracted and peaks corresponding to the J/ψ, ψ', $\Upsilon(1S, 2S, 3S)$ have revealed. Blue colored is the continuum spectrum described by correlated heavy flavour from D meson and beauty B. Other estimate coming from Drell-Yan contributions estimated using a PYTHIA simulation includes the detector acceptance and efficiencies. The spectrum is dependent on dielectron yield scaled to the invariant mass. The correlated $c\bar{c}$ and $b\bar{b}$ blue line and Drell-Yan decreasing trend can be concluded.

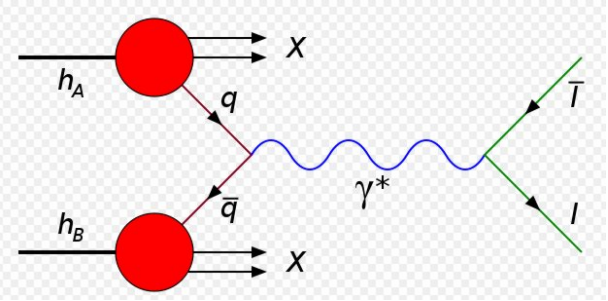

Figure 7.6: Drell-Yan

The Drell–Yan process mentioned earlier (Fig.7.6) occurs in high energy hadron–hadron scattering. It takes place when a quark of one hadron and an antiquark of another (anti-) hadron annihilate, creating a virtual photon or Z

boson which then decays into a pair of oppositely-charged leptons.The main observable is the forward–backward asymmetry in the angular distribution of the two leptons in their center-of-mass frame [14] [15] .

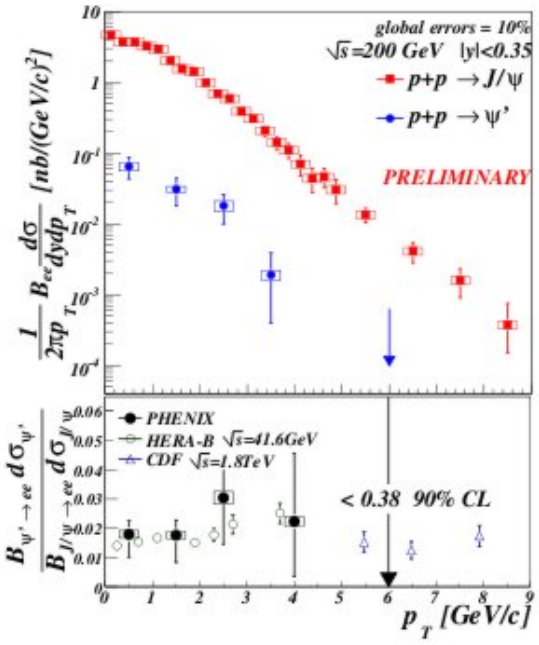

Figure 7.7: Transverse momentum dependence

The ψ' differential cross section shown in Fig.7.7 is the first p_T-dependent result for an excited charmonium state at RHIC. There is also shown and compared ψ' to J/ψ ratio to the results from HERA-B and CDF. The differential cross section and transverse momentum are logarithmically scaled. The numbers are well in agreement with average results but in higher p_T there the error has been decreased while the global error is about 10%. It can be concluded that differential cross section of both production decreases with growing p_T meanwhile ψ's to J/ψ ratio is still around 0.02 and it is less than 0.38 with 90% CL (limit). That means no value of this ratio could be measured as higher than 0.38 with 90% probability. This is called up-to-date feed-down contributions: to J/ψ from ψ' it is $8.6 + -2.5\%$.

The J/ψ p_T distributions in p+p and Cu+Cu collisions at $\sqrt{s_{NN}} = 200GeV$ measured by STAR is shown(Fig.7.8 left). Also shown are perturbative calculations for LO CS+CO (solid line) and NNLO* CS (band) direct yields, without feed-down contributions.

The LO denotes the leading order calculations to estimate cross section.

The NNLO is used for corrections of produced cross section of final partons where the processes like gluon or quark radiation, gluon splitting or the flavor excitation are included. The CO+CS mean the color octet model and the color singlet model. The charmonium can emerge from the hard interaction either immediately with the right values of spin, angular momentum and color (CS) or in a colored $c\bar{c}$ state (CO), which is followed by a long distance transition to charmonium and light hadrons.

On Fig.7.8 the measured $J/\psi \longrightarrow e^+e^-$ p_T spectra are presented. The systematic uncertainties are dominated by kinematic cuts, trigger efficiency (9%) and reconstruction efficiency (8%), and are similar and correlated in p+p and Cu+Cu. The normalization uncertainty for the inclusive non-singly diffractive p+p cross section is 14% [11] [12] [13] . Theoretical calculations shown in the figure are NRQCD from CO and CS transitions for direct J/ψ's in p+p collisions (solid line) and NNLO CS result (gray band). Neither calculation includes feed-down contributions. The band for NNLO gives the uncertainty due to scale parameters and the charm quark mass. The CS+CO calculation describes the data well and leaves little room for feeddown from ψ', χ_c and B, estimated to be a factor of ≈ 1.5. NNLO CS predicts a steeper p_T dependence.

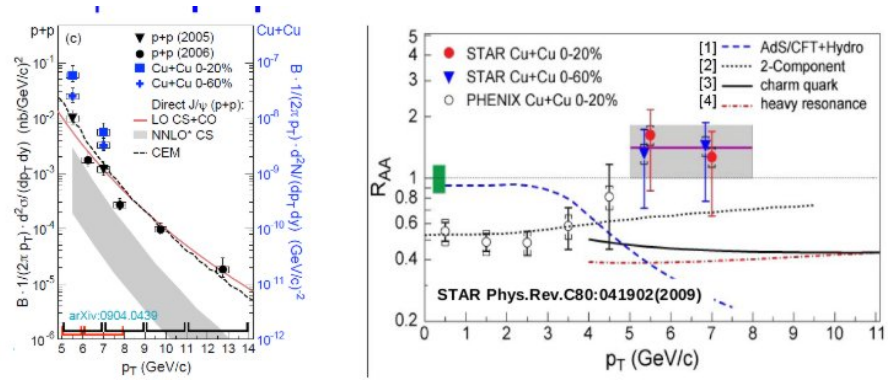

Figure 7.8: Rapidity dependence of the modification factor and comparison from parton modification distributions

The modification factor R_{AA} vs. p_T of J/ψ is presented in Fig.7.8, right. STAR data points have statistical (bars) and systematic (caps) uncertainties. The box about unity on the left shows R_{AA} normalization uncertainty. The solid line and band show the average and uncertainty of the two $0-20\%$ data points. The curves are model calculations described in the text. The uncertainty band of 10% for the dotted curve is not shown.

From these data J/ψ is the only hadron measured in RHIC heavy-ion collisions that does not exhibit significant high p_T suppression. For the J/ψ population, the initial scattered partons have average momentum fraction ≈ 0.1. The initial state effects such as anti-shadowing may lead to increasing R_{AA} with

increasing p_T .The dashed curve in Fig.7.8 (right) shows the prediction of an AdS/CFT-based calculation, in which the J/ψ is embedded in a hydrodynamic model [8] and the J/ψ dissociation temperature decreases with increasing velocity. Its p_T dependence is at variance with that of the data. The dotted line shows the prediction of a two-component model including color screening, hadronic phase dissociation, statistical $c\bar{c}$ coalescence at the hadronization transition, J/ψ formation time effects, and B-meson feed-down [9].

The other calculations in Fig.7.8 (right) provide a comparison to open charm R_{AA}. The solid line is based on the WHDG model for charm quark energy loss, with assumed medium gluon density $dNg/dy = 254$ for $0 - 20\%$ Cu+Cu.

The dash-dotted line shows a GLV model calculation for D-meson energy loss, with $dNg/dy = 275$. Both models correctly describe heavy-flavor suppression in Au+Au collisions. They predict charm meson suppression of a factor ≈ 2 at $p_T > 5GeV/c$. This is in contrast to the J/ψ R_{AA}. This comparison suggests that high-p_T J/ψ production does not proceed dominantly via a channel carrying color. However, other effects may compensate for the predicted loss in this p_T range [10].

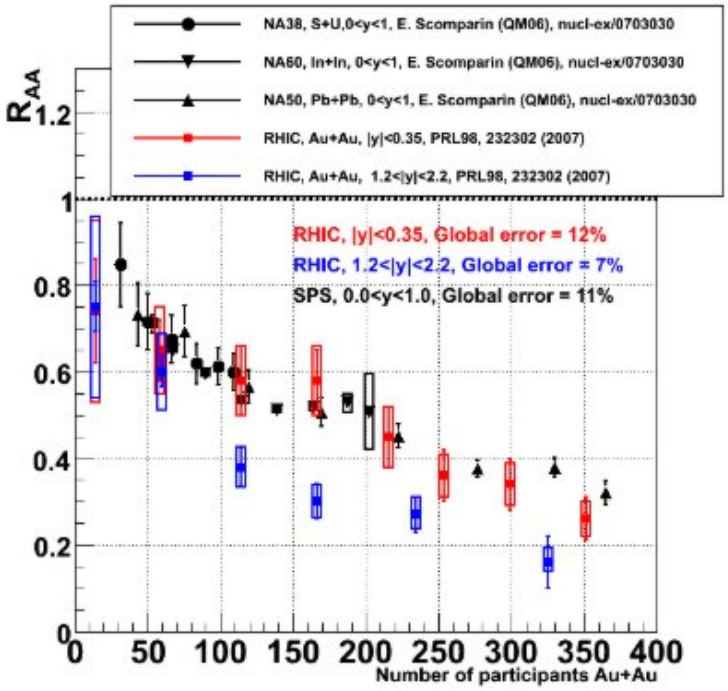

Figure 7.9: The function of modification factor to number of participants. RHIC and SPS measurement of different midrapidity.

On Fig.7.9 R_{AA} of J/ψ is shown as function of number of participants in collision of SPS and RHIC. It is a puzzle that suppression is at the same strength although energy at collisions is very different.

In the rest of the chapter we discussed other quarkonia system, Upsilon.

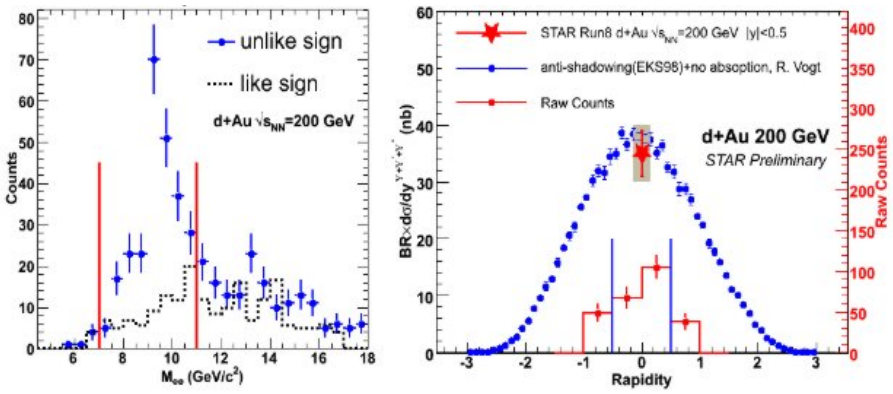

Figure 7.10: d-Au collisions, dieclectron invariant mass and rapidity distribution

On Fig.7.10 the dielectron invariant mass in Upsilon mass region measured by STAR is shown for $d + Au$ collision at $\sqrt{s_{NN}} = 200GeV$. In Fig.7.10 right, the rapidity distribution of measured Υ is shown and also yield of $\Upsilon \rightarrow e^+e^-$ at midrapidity.

Unlike-sign raw yield N_{+-} (filled circles) in the region $|y_{ee}| < 0.5$, where y_{ee} is the pairwise rapidity, and like-sign combinatorial background $2\sqrt{N_{++}N_{--}}$ (line histogram). The background is fit to an exponential multiplied with an error function from the STAR Υ trigger (dashed line).

The STAR measurement of the midrapidity $\Upsilon(1S + 2S + 3S)$ cross section times branching ratio into electrons (star). Error bars are statistical, the box shows the systematic uncertainty, and the scale is given by the left axis. The raw yield vs. y is shown by the histogram at the bottom (diagonal-line fill pattern), with scale on the right axis. The cross section was calculated from the yield between the vertical dot-dashed lines, $|y_{ee}| < 0.5$. The open squares are from an NLO CEM calculation, and the two dotted lines give the limits for the prediction from a NLO CSM calculation of the Υ cross section. Evolution of the $\Upsilon(1S + 2S + 3S)$ cross section with center-of-mass energy from STAR with statistical and systematic errors is presented as in Fig.7.11. [4] [5] [6] [7] The symmetry for accepting unlike-sign and like-sign pairs makes the ratio of acceptances unity, so the only $2\sqrt{N_{++}N_{--}}$ for the combinatorial background is used.

The measurement of Υ production in $p+p$ at $\sqrt{s_{NN}} = 200GeV$ by STAR is shown. The result is obtained for the cross section is shown in Fig.7.11(down-left) from the STAR measurement. The error bars and the box depict the statistical and systematic uncertainties. To illustrate the acceptance in rapidity

there is also shown the unlike-sign pairs after like-sign background subtraction, $N_{+-} - 2\sqrt{N_{++}N_{--}}$, in the Υ region $8 < m_{ee} < 11GeV/c^2$ as a hashed histogram. The scale on the right axis of the figure is used for the counts in the histogram, and the scale in the left axis of the figure is used for the cross section. The measurement with NLO CEM predictions is compared [6] of the $\Upsilon(1S)$ rapidity distribution.

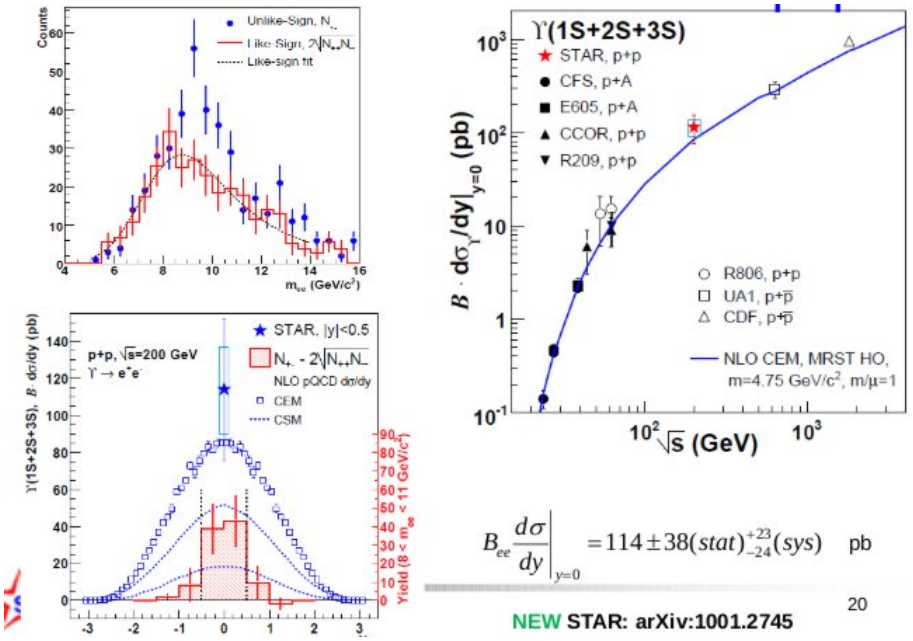

Figure 7.11: The STAR measurement of the midrapidity $\Upsilon(1S+2S+3S)$ cross section

Since have been measured all three states and only in the dielectron channel, the calculation of the $\Upsilon(1S)$ is scaled by a factor

$$\frac{\vec{B}(1S) \times \sigma(1S) + \vec{B}(2S) \times \sigma(2S) + \vec{B}(3S) \times \sigma(3S)}{\sigma(1S)} \tag{7.3}$$

in order to compare it to measurement of the cross section for all three states. The calculation is in agreement with this measurement. The two dotted lines in the plot are the upper and lower bounds of the cross section obtained from a calculation in the CSM for direct $\Upsilon(1S)$ production [7] based on NLO code developed for quarkonium production at hadron colliders.

Fig.7.11 (down-left): The STAR measurement of the midrapidity $\Upsilon(1S + 2S + 3S)$ cross section times branching ratio into electrons (star) is given. The raw yield vs. y is shown by the histogram at the bottom (diagonal-line fill pattern), with scale on the right axis. The cross section was calculated from the

yield between the vertical dot-dashed lines, $|y_{ee}| < 0.5$. The open squares are from an NLO CEM calculation, and the two dotted lines give the limits for the prediction from a NLO CSM calculation of the Υ cross section [5].

Since the calculation is for the 1S state alone and for direct Υ production (ignoring feed-down from P-states). To compare this measurement which includes all 3 states and feed-down contributions, the values from the calculation were divided by a factor 0.42 to account for this. The bounds in the calculation are obtained by varying the bottom quark mass and the renormalization and factorization scales. The CSM prediction is lower than the data, indicating that additional contributions are needed beside production via color singlet.

In Fig.7.11 (right) there is also compared $\Upsilon(1S+2S+3S)$ result with measurements done in $p+A$, $p+p$ and $p+\bar{p}$ collisions at center-of-mass energies ranging from 20 GeV up to 1.8 TeV, and to NLO CEM predictions [6] for a wide range of center-of-mass energies. This is consistent with the overall trend, and provides a reference for bottomonium production at the top RHIC energy.

The STAR experiment has measured the $\Upsilon(1S+2S+3S) \longrightarrow e^+e^-$ cross section at midrapidity , $|y_{ee}| < 0.5$, in $p+p$ collisions at $\sqrt{s} = 200GeV$ to be $(\vec{B} \times d\sigma/dy)^{1S+2S+3S} = 114 \pm 38$ (stat.)$^{+23}_{-24}$ (syst.)pb. Calculations done in the Color Evaporation Model at NLO are in agreement with measurement, while calculations in the Color Singlet Model underestimate cross section. However, this is only a $\approx 2\sigma$ effect with the present statistics. A combined continuum cross section, Drell-Yan plus $b-\bar{b} \longrightarrow e^+e^-$, measured in the kinematic range $|y_{ee}| < 0.5$ and $8 < m_{ee} < 11GeV/c^2$, of $(\sigma_{DY} + \sigma_{b-\bar{b}}) = 38 \pm 24$ pb were reported.

The STAR measurement presented here will be used as a baseline for studying cold and hot nuclear matter effects in d+Au and Au+Au collisions. With increased luminosity, a better determination of the cross section, its p_T dependence and a separation of the 2S and 3S states will be possible. The projected luminosity upgrades to RHIC should increase the Υ yield to ≈ 8300 in $p+p$ and ≈ 11200 in $Au+Au$ collisions during one RHIC year. The increased statistics will reduce the uncertainty in the determination of the continuum cross section and will allow a thorough study of the bottomonium sector by resolving the 2S and 3S states [3].

Chapter 8

Summary

In summary, RHIC program have produced multiple interesting observations of QGP. One of important measurements are in heavy flavor sector. These measurements put the constrains to understanding of properties of nuclear matter. More direct measurement in open heavy sector is needed to address more precisely charm cross section.

Nuclear modification factor of Upsilon at RHIC and LHC will put a distinct constrains to temperature of created matter. New era of nucleus-nucleus collision at LHC will allow to conclude in understanding to QGP.

Bibliography

[1] A. Adare et al. (PHENIX Collaboration), Phys. Rev. Lett. 98, 232301 (2007).

[2] J.C. Dunlop, Open Heavy Flavor Production in Heavy Ion Collisions, a Brookhaven National Laboratory, Upton, NY, 11973, USA.

[3] B. I. Abelev, Upsilon cross section in $p + p$ collisions at $\sqrt{s} = 200GeV$, arXiv:1001.2745v1 [nucl-ex] (15 Jan 2010).

[4] M. C. Abreu et al., Eur. Phys. J. C 14, 443 (2000).

[5] J. M. Campbell, F. Maltoni and F. Tramontano, Phys. Rev. Lett. 98, 252002 (2007).

[6] A.D. Frawley, T. Ullrich and R. Vogt, Phys. Rept. 462, 125 (2008).

[7] S. J. Brodsky and J. P. Lansberg, arXiv:0908.0754 [hepph].

[8] T. Gunji, J. Phys.G: Nucl. Part. Phys. 35, 104137 (2008).

[9] X. Zhao and R. Rapp (2007), arXiv:0712.2407.

[10] B.I. Abelev, J/ψ production at high transverse momenta in pp and $CuCu$ collisions, arXiv:0904.0439v1 [nucl-ex] 2 Apr 2009.

[11] J. Adams et al., Phys. Rev. Lett. 91, 172302 (2003).

[12] G. C. Nayak, M. X. Liu, and F. Cooper, Phys. Rev. D68, 034003 (2003).

[13] P. Artoisenet et al., Phys. Rev. Lett. 101, 152001 (2008).

[14] S.D. Drell, T.-M. Yan: Massive Lepton-Pair Production in Hadron-Hadron Collisions at High Energies, PhysRevLett.25.316 (1970).

[15] J.H. Christenton, G.S. Hicks, L.M. Lederman, P.J. Limon, B.G. Pope, E. Zavatinni: Observation of Massive Muon Pairs in Hadron Collisions, PhysRevLett.25.1523 (1970).

[16] Matsui, T; Satz, H: J/ψ suppression by quark-gluon plasma formation, Physics Letters B 178: 416 (1986).

[17] Thews, RL; Schroedter, M; Rafelski, J: Enhanced J/ψ production in deconfined quark matter, ariv:hep-ph/0007323 (2001).

[18] Schroedter, M; Thews, RL; Rafelski, J: B_c-meson production in ultrarelativistic nuclear collisions, Physical Review C 62: 024905. doi:10.1103/PhysRevC.62.024905. ariv:hep-ph/0004041 (2000).

[19] Fulcher, LP; Rafelski, J; Thews, RL: B_c mesons as a signal of deconfinement, ariv:hep-ph/9905201 [hep-ph] (1999).